Journal of Cleaner Production 331 (2022) 129920

Contents lists available at ScienceDirect

Journal of Cleaner Production

journal homepage: www.elsevier.com/locate/jclepro

Ensemble transfer learning for cutting energy consumption prediction of aviation parts towards green manufacturing

Fengyi Lu [a], Guanghui Zhou [a,b,**], Yang Liu [c,d,*], Chao Zhang [a,b]

[a] School of Mechanical Engineering, Xi'an Jiaotong University, Xi'an, 710049, China
[b] State Key Laboratory for Manufacturing Systems Engineering, Xi'an Jiaotong University, Xi'an, 710054, China
[c] Department of Management and Engineering, Linköping University, SE-581 83 Linköping, Sweden
[d] Department of Production, University of Vaasa, 65200 Vaasa, Finland

ARTICLE INFO

Handling editor: Cecilia Maria Villas Bôas de Almeida

Keywords:
Green manufacturing
Cutting energy consumption prediction
Ensemble transfer learning
Bayesian-MCMC calibration

ABSTRACT

Cutting energy consumption prediction gives decision supports for the energy-saving operation to realise green manufacturing. However, there are challenges when predicting aviation parts due to the machining features causing tool wear and expensive data labelling. Consequently, this paper builds a prediction model and emphasises training with limited experimental data by proposing an ensemble transfer learning approach. The approach incorporates transfer learning, i.e., TrAdaBoost-R2 (TR) algorithm, and calibration, i.e., Bayesian and Markov chain Monte Carlo calibration (MCMC). Firstly, a cutting energy consumption prediction model considering tool wear is formulated with cutting and tool parameters as the inputs. Secondly, a dataset including experiment and simulation data for training is constructed, where TR is used to identify the valuable data from the simulation model calibrated by MCMC. Then random forest regression (RFR) is introduced as a base learner to train the prediction model on the hybrid dataset. Finally, a case study of the aluminium alloy 7075 parts milling process shows that the proposed method is accurate in cutting energy consumption prediction. Compared with RFR and TR-RFR, the proposed method's coefficient of determination (R2) increases by 11.60% and 3.55%, indicating high goodness of fit under the same small samples of the experiment. Therefore, the proposed method could help determine the most efficient process plan without excessive time, materials and energy, significantly contributing to green manufacturing.

1. Introduction

Energy consumption prediction of parts manufacturing is a critical consideration to achieve green manufacturing. According to Ali et al. (2019), the machining energy consumption generated by the aeronautical parts accounts for about 34% of the aerospace industry. Among them, cutting energy consumption accounts for around 60% of energy consumption in the machining process (Hu et al., 2017b). This reveals the energy-saving potential of cutting states for aero-parts. Therefore, to improve the machining energy efficiency of aviation parts, it is necessary to reduce the related cutting energy consumption (Gialos et al., 2018). Considering this, cutting energy consumption prediction of aviation parts should be regarded as a crucial prerequisite. It can assist in assessing several process plan alternatives based on the impact of cutting energy consumption towards aviation green manufacturing (Lv et al., 2020).

Aviation parts made of aluminium, titanium, and composite materials have good properties, i.e., lightweight, high specific strength, and good corrosion resistance (Chen et al., 2021). Among them, aluminium alloy 7075 is famous for its easy forming of various shapes (Kaczyński et al., 2020). Nevertheless, the cutting energy consumption prediction for parts made of such material is difficult as the complex machining process involves many variables (Pereira et al., 2017). Other challenges are costly data acquisition and high energy consumption that is accompanied by tool wear due to the mechanical strength of the material (Luo et al., 2021). This has contributed to difficulties in accurately predicting cutting energy consumption and the inability to support sustainable optimisation in process planning.

Aiming to work out such a prediction dilemma, explorations are performed in state-of-the-art literature related to cutting energy consumption of aero-part and other manufacturing fields. Among them, the

* Corresponding author. Department of Management and Engineering, Linköping University, SE-581 83 Linköping, Sweden.
** Corresponding author. School of Mechanical Engineering, Xi'an Jiaotong University, No.28 Xianning West Road, Xi'an, 710049, China.
E-mail addresses: luke0612@stu.xjtu.edu.cn (F. Lu), ghzhou@mail.xjtu.edu.cn (G. Zhou), yang.liu@liu.se (Y. Liu), superzc@xjtu.edu.cn (C. Zhang).

https://doi.org/10.1016/j.jclepro.2021.129920
Received 19 June 2021; Received in revised form 22 November 2021; Accepted 26 November 2021
Available online 1 December 2021

Nomenclature

E_e, E_{basic}, E_{aircut}, E_{cut}	total, basic, air cutting and cutting energy consumption of one working step of machine tool
P_{basic}, P_{aircut}, P_{cut}	basic, air-cutting and cutting power
t_{basic}, t_{aircut}, t_{cut}	time of the basic,air-cutting and cutting stages
t_{ra}, t_{re}, t_h, t_d	rake, relief, helix angle and tool diameter
c_d, c_w, fr, n	cutting depth, cutting width, feed rate and spindle speed
T_{src}, T_{tar}	simulation and experiment datasets
w_i^{t+1}	the weights of T_{tar} and T_{src}
P^t	the trained model at tth iteration
z_t	normalised constant
β,β_t	weight coefficients of T_{tar} and T_{src}
e_i	average loss of P^t on the T_{tar}
e_i^t	loss function of the base learner on the T_{tar} at tth iteration
f_t	predicted value of the learner
A,B,C	yield stress of the material, strain hardening constant and strain coefficient
v_f,v_r,v_s	cutting speed, rotary speed of the cutting tool and sliding speed
F, F_{cut}, F_N	resultant cutting force, basic cutting force and axial force
θ, β	instantaneous and maximum milling angles
L	working path length per tooth
n	cutter tooth number
ω	angular velocity
P_{rc}, P_{ac}	resultant and additional cutting power
F_{tw}, F_{zw}	frictional and tangential force
vb^*	fixed length of elastic contact area
vb	tool wear that occurs on the flank surface
σ_n	normal pressure
A_c, B_c	constants in Usui's model
α_x, α_y, Δe	coefficients to be calibrated
Y_i, Y_i'	actual and theoretical values of the ith samples
T_d, T_0, T_{melt} T_{int}	deformation, room melting and interface temperature

web of science is used as the search database for its broader coverage. The searching keywords and process are presented in Table 1, the related works are summarised in Table 2.

The machining energy consumption of a machine tool can be divided into two types: cutting energy consumption and non-cutting energy consumption (Hu et al., 2017a). The cutting energy consumption in Hu et al. (2017b) denotes the energy exhausted from the net cutting states, which is related to process parameters. Wang et al. (2016) modelled the specific energy consumption of 7050-T7451 aluminium alloy in high-speed machining, considering tool rake angles and cutting speed. Bolar et al. (2018) presented a cutting force mathematical model of aviation aluminium alloy with cutting parameters, which proved high accuracy. Dahbi et al. (2017) studied prediction for characterising the cutting force and power considering cutting parameters and tool radius. These most focused on empirical modelling for cutting force or power and proved a strong correlation between cutting conditions and cutting force or energy. Still, these attempts did not go far enough to provide any technological means to deal with the expensive data-labelling and highly nonlinear prediction dilemma.

Scholars have proposed many prediction methods in the parts machining made of common materials, laying the foundation for this problem. According to whether to rely on qualitative experience and model, there are two ways to realise the machining energy consumption prediction: formalised model-based or data-driven technology. The first type refers to the establishment of the formalised model using methods as Petri net (Wang et al., 2019), ontology-based modelling (Zhou et al., 2017), cutting force modelling (Shi et al., 2019), specific-energy modelling (Deng et al., 2017) and energy consumption empirical modelling (Khan et al., 2020). However, such methods tend to show poor performance when the machine tools and operating conditions are uncertain, and the prediction problem is of high dimension.

By contrast, many adopted data-driven methods to research with a better approximation ability for nonlinear prediction (Tong et al., 2021). At present, more widely used neural networks like artificial neural networks, i.e., ANNs (Arafat et al., 2020) and convolutional neural networks, i.e., CNNs (He et al., 2020), and machine learning, e.g., random forest regression (RFR), to solve regression problems (Li et al., 2018). However, training ANNs require the estimation of values for numerous parameters that may affect the robustness of the model (Rodriguez-Galiano et al., 2015). For this reason, RFR is getting valued for its strong nonlinear mapping ability, good generalisation characteristics and few parameters. Therefore, it is preferred in this paper considering the complex machining features of aero parts.

To sum up, those state-of-the-art works prove a strong relationship between cutting conditions and cutting energy consumption and provide theoretical and method references. However, it is far from enough to cope with the prediction problem of aero-parts machining with the existing methods well, and the gaps are summarised below:

(1) Formalised models have been widely adopted in the literature to predict the energy consumption of the machining process. However, the models will find their limited reliabilities when applied to aero parts prediction, as the model parameters are hard to be determined due to the high dimension of the machining.
(2) By contrast, standard data-driven methods are preferred. However, such methods, including the RFR algorithm, all exceptionally rely on sufficient historical data (Deng et al., 2021; Chen et al., 2020; Hong et al., 2020; Lin et al., 2020). Unfortunately, it tends to be unacceptable for aviation parts to perform costly and time-consuming data collection, limiting the application of green manufacturing in the aviation field.

Motivated by insufficiencies, the transfer learning algorithm (Dai et al., 2007) is introduced. It is a promising approach to overcome the difficulties of the data-driven methods in training by using the knowledge gained in similar domains. However, if the data from a similar domain contains too much noise, the negative model transfer may exist (Niu et al., 2020). Therefore, an ensemble transfer learning method is proposed for predicting the cutting energy consumption of aviation parts. A novel transfer learning regression reduces the training experiment samples by the ensemble ideas of "transfer" and "calibration". First of all, simulation and experiment are viewed as the source and target domains. Then, the "Transfer" uses TrAdaBoost-R2 (TR) (Lv et al., 2019) and takes a base learner, RFR algorithm, to facilitate the improvement for model training via transferring valuable simulation knowledge. As an instance-based transfer learning, TR permits the source domain with

Table 1
Summary of searching keywords and process used for this literature review.

Literature search strings	Search fields	Limit to
("aviation parts" OR "aluminium alloy" OR "titanium alloy") AND ("cutting energy consumption" OR "cutting force" OR "cutting power") AND (prediction OR model)	Subject	Engineering, English
("cutting energy consumption" OR "machining energy consumption") AND (model OR prediction)	Subject	Engineering, English

Table 2
Summary of previous studies related to cutting energy consumption of aero-parts.

References	Type of quantification		Tool wear impacts		Prediction for aero-parts		Demand
	Formalised type	Data-driven type	Yes	No	Yes	No	
Wang et al. (2016)	✓			✓	✓		Empirical model of specific energy consumption
Bolar et al. (2018)	✓			✓	✓		Empirical model of cutting power
Dahbi et al. (2017)		✓		✓	✓		Large amount of actual data and model parameters for cutting force
Wang et al. (2019)	✓			✓		✓	Empirical model and knowledge rules of energy consumption
Zhou et al. (2017)	✓			✓		✓	Carbon emissions-process bill of material of cutting tool
Shi et al. (2019)	✓			✓		✓	Empirical model of cutting power
Deng et al. (2017)	✓			✓		✓	Empirical model of cutting specific energy consumption
Khan et al. (2020)	✓			✓		✓	Empirical model of cost and energy consumption
Tian et al. (2019)	✓		✓			✓	Empirical model taking tool wear as inputs
Arafat et al. (2020)		✓		✓		✓	Large amount of actual data and model parameters
He et al. (2020)		✓		✓		✓	Large amount of actual data and model parameters
Li et al. (2018)		✓		✓		✓	Large amount of actual data but few model parameters
This paper		✓	✓		✓		Small amount of actual data and few model parameters

distributions different from the target. Meanwhile, the "Calibration" borrows the idea of Bayesian-Markov chain Monte Carlo (MCMC), a statistical inference method (Xu et al., 2018), to reduce uncertainties of the simulation that may cause possible data noise.

Firstly, to realise the method, a cutting energy-consumption prediction model considering tool wear is formulated with cutting and tool parameters inputs. Then, the simulation model and experiment are used for data collection. Subsequently, the Bayesian-MCMC is applied to calibrate the simulation model. Then, the TR based on RFR uses limited experimental data and rich calibrated simulation data to train the prediction model. Compared with previous work, its main novelties include:

- It proposes a data-driven prediction model of the cutting energy consumption for aviation parts considering the impacts of tool wear;
- It attempts to overcome the costly and energy wastes in data labelling by using transferring to leverage simulation data and focuses on avoiding negative transfer and data noise by utilising Bayesian-MCMC;
- Good prediction accuracy and sensitive analysis provide instructions for the aviation industry to select the optimal energy-saving process plans.

To the best of our knowledge, this method is firstly proposed for cutting energy prediction of aero-parts manufacturing, providing decision-supports of energy-saving process plans, thus improving the sustainability of aerospace manufacturing. The method performs well in a case study of aluminium alloy 7075 parts milling.

The organisation of this paper is as follows: Section 2 presents a prediction model of cutting energy consumption. In Section 3, the proposed ensemble transfer learning method, including transfer, calibration and training mechanism, is elaborated. After obtaining the required data, the applicability and performance of the proposed method are verified in Section 4. Finally, Section 5 concludes this paper and offers future research directions.

2. Overview of the proposed approach

This section discusses the research problem and formulates a prediction model, providing a training basis for the proposed method.

2.1. Problem description

First of all, the focus is on the cutting stage of aero parts. Considering one specified part having different features and corresponding processes, cutting energy consumption E_{cut} is quantified from one working step in one process of one feature, shown in Fig. 1.

From Fig. 1, the energy consumption of one working step is formalised as expressed in Eq. (1).

$$\begin{aligned} E &= E_{basic} + E_{aircut} + E_{cut} \\ &= P_{basic} \cdot t_{basic} + P_{aircut} \cdot t_{aircut} + P_{cut} \cdot t_{cut} \end{aligned} \tag{1}$$

where P_{basic} refers to the basic power, including start, standby, idle and other basic stages of the machine tool. P_{aircut} refers to the air-cutting power of the machine tool, P_{cut} refers to the cutting power of machining parts, t refers to the time experienced by each stage.

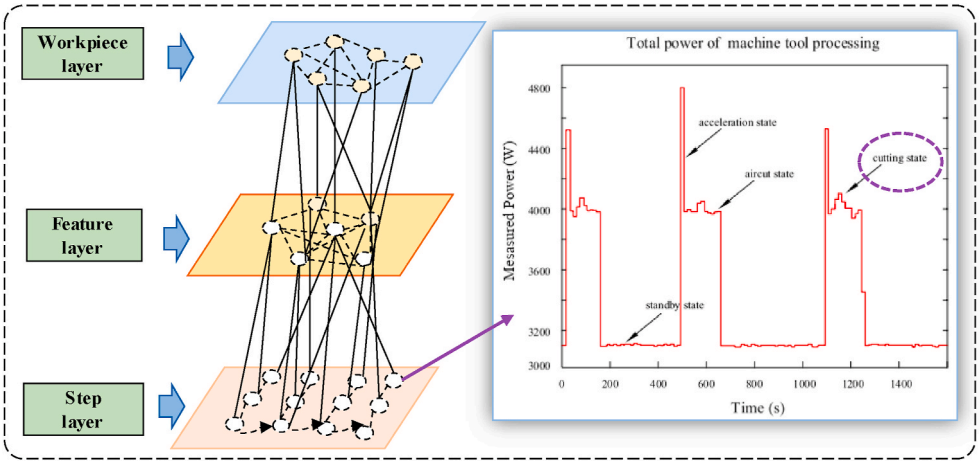

Fig. 1. Quantification idea for cutting energy consumption.

According to Eq. (1), E_{basic} and E_{aircut} can be acquired easily by utilising the data of P_{basic} and P_{aircut} from established databases for a specific machine tool. Conversely, there is almost no fixed model that can render itself supportive of calculating the E_{cut} directly. Considering the energy-saving optimisation potentials (Xu et al., 2020), the focus falls on the quantification of E_{cut}. Therefore, this research is dedicated to solving the quantification problem of net cutting energy consumption of aero parts. So, the prediction begins from material removal with the input of electricity and ends up with the completion of a working step feature.

2.2. Model formulation

The prediction model adopts an "Input/Output" mode. Based on previous work (Wang et al., 2016; Liu and Zong, 2019) and preliminary trial runs, taking milling process as an example, factors that influence cutting energy consumption and tool wear are selected as inputs, including tool parameters, i.e., rake angle t_{ra}, relief angle t_{re}, tool diameter t_d and helix angle t_h, and cutting parameters, i.e., cutting depth c_d, cutting width c_w, feed rate f_r and spindle speed n. P_{cut} is denoted as output that is finally transformed into E_{cut} based on Eq. (1). The model is expressed as:

$$\begin{aligned} &\text{Objective}: E_{cut} \\ &Input: x_{tp}(t_{ra}, t_{re}, t_d, t_h), x_{cp}(c_d, c_w, f_r, n) \\ &Output: P_{cut} \\ &Subject\ \ to: x_L \le x_{tp}, x_{cp} \le x_U \end{aligned} \tag{2}$$

where x_{tp} is denoted as tool parameters, x_{cp} is denoted as cutting parameters, x_L and x_u denote the lower and upper bounds. To solve the model, the training process is shown in Fig. 2.

From Fig. 2, it is found that the learning method and data needed by the training model count for much. Although there are many ways to realise prediction, only a small amount of data is available for model training in actual experiments when sustainability and energy saving become the primary concerns. Thus, to achieve high accuracy without sacrificing the environment, an ensemble approach is proposed, and the main idea is elaborated in Section 3.

3. Ensemble approaches for model training

This study proposes an ensemble strategy of transfer learning, machining learning, and Bayesian calibration for cutting energy consumption prediction where aluminium alloy 7075 parts milling is studied. The basic idea is illustrated in Fig. 3.

From Fig. 3, the idea mainly consists of two steps: (1) dataset construction; (2) learning algorithm for training the model. In step (1), a hybrid dataset is built containing data from simulation and experiments. To reduce the uncertainties of the simulation data, the Bayesian-MCMC calibration is used. After that, TR boosts a basic learner by reusing the calibrated simulation data that is most similar to the experiment data. In step (2), RFR is selected as the learner to model complex interactions among input variables. By calibration and transferring, the ensemble method could improve prediction accuracy and alleviate the costly data-acquisition problem.

3.1. Dataset construction and transfer mechanism

3.1.1. Transfer learning mechanism

The costly data acquisition of aviation parts in the machining process impedes high accuracy prediction of the data-driven algorithms. To deal with such drawbacks, transfer learning is adopted. In detail, the idea behinds transfer learning is that it is easier to learn a new rule if a similar rule is obtained by using knowledge, thus improving the learning performance by avoiding expensive data-labelling efforts. TR is chosen as the transfer learning approach to add the simulation knowledge into the experiment in an adaptive-weighted updating way so that the simulation knowledge can be leveraged to the utmost (Xu and Meng, 2020).

Suppose there is a hybrid training dataset $T = T_{src} \cup T_{tar}$, where $T_{src}=\{(x_i^n, y_i^n)\}$ denotes the simulated dataset with the size of n and $T_{tar}=\{(x_j^m, y_j^m)\}$ denotes the experiment dataset with the size of m, both datasets are offered with weight distributions as Eq. (3):

$$w^1 = \left(w_1^1, \ldots, w_{n+m}^1\right), w_i^1 = \frac{1}{n+m}, i \in (1, n+m) \tag{3}$$

Define maximum iterations number as M, the model P^t is trained on the dataset T with a base learner at t^{th} iteration, and the weights of T_{tar} and T_{src} are updated respectively as Eq. (4).

$$w_i^{t+1} = \begin{cases} \dfrac{w_i^t \beta^{|f_t(x_i)-y_i|}}{z_t}, & i \in (1, n) \\ \dfrac{w_i^t \beta^{-|f_t(x_i)-y_i|}}{z_t}, & i \in (n+1, \cdots, n+m) \end{cases} \tag{4}$$

where z_t is a normalised constant to make sure the sum of w_i^{t+1} is 1, β and β_t are the weight coefficients of T_{tar} and T_{src}:

$$\beta = 1 \Big/ \left(1 + \sqrt{2In\left(\frac{n}{m}\right)}\right) \tag{5}$$

$$\beta_t = \frac{\varepsilon_i}{1-\varepsilon_i} \tag{6}$$

where ε_i is the average loss of P^t on the T_{tar} as expressed in Eq. (7).

$$\varepsilon_i = \sum_{i=n+1}^{n+m} \frac{w_i^t e_i^t}{\sum_{i=n+1}^{n+m} w_i^t} \tag{7}$$

where e_i^t is the loss function of the base learner on the T_{tar} at t^{th} iteration:

$$e_i^t = \left|\frac{(f_t(x_i) - y_i)^2}{D}\right|, i \in (n+1, n+m) \tag{8}$$

$$D = \max_{i \in (n+1, n+m)} (f_t(x_i) - y_i) \tag{9}$$

where f_t is the predicted value of the learner.

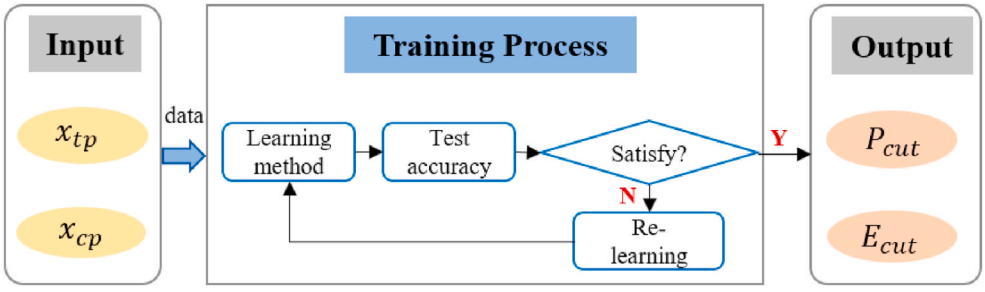

Fig. 2. The training process.

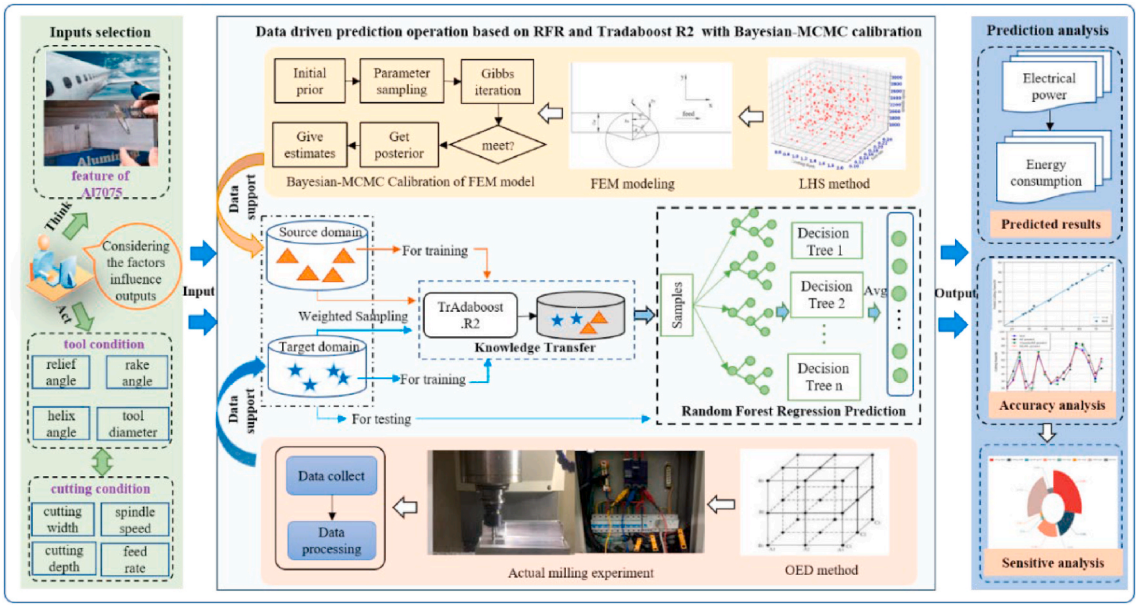

Fig. 3. The workflow of the proposed strategy.

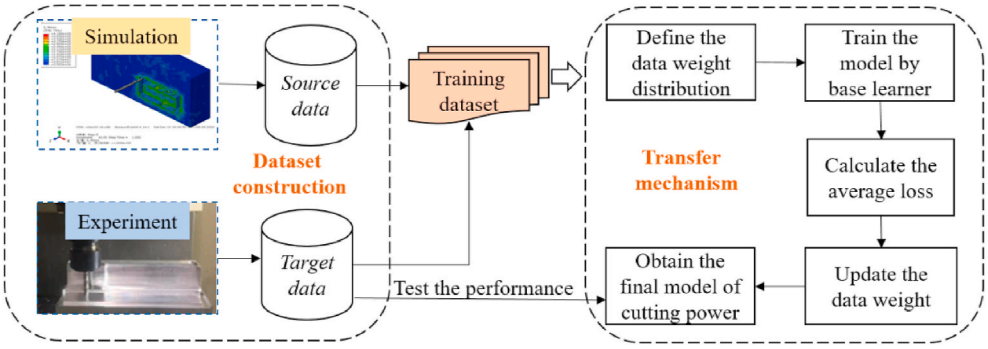

Fig. 4. The transfer learning mechanism of this study.

During transfer learning, the weights of source data with large errors are reduced in the next iteration to lower its impact on the prediction model. Instead, the target data receives more attention by increasing its weight. In such a way, the source data would be exploited effectively. The transfer learning mechanism is shown in Fig. 4.

3.1.2. Simulation dataset construction with Bayesian-MCMC calibration

Finite element analysis (FEA) is a physics-computational simulation for complex physical systems used in many fields because of its convenience and relatively good precision (Wimmer et al., 2019). FEA is carried out for the dataset construction to model the milling process of aluminium alloy 7075 parts. Moreover, Latin Hypercube Sampling (LHS) is adopted as it can approximately sample multivariate parameters (Wang et al., 2020a).

A Johnson-Cook material model is used during FEA modelling as the workpiece material model represented by Eq. (10).

$$\sigma = [A + B(\varepsilon)^n] \cdot \left[1 + C\ln\left(\frac{\dot{\varepsilon}}{\dot{\varepsilon}_o}\right)\right] \cdot \left[1 - \left(\frac{T - T_o}{T_{melt} - T_o}\right)^m\right] \tag{10}$$

where A is the yield stress of the material; B is the strain hardening constant; C is the strain coefficient; n is the strain hardening effect; m is the thermal softening effect; T_d is the deformation temperature; T_0 is the room temperature; T_{melt} is the melting point temperature of the material.

Afterwards, the mechanical and physical properties of the material are shown in Table 3, and unknown parameters of the Jonson-Cook model are determined in Table 4. Finally, the milling process is expressed to simulate the cutting force to obtain the results.

Table 3
Mechanical and physical properties for aluminum alloy 7075.

Properties	Conductivity (W/(m·K))	Expansion (10^{-5})	Elastic modulus (GPa)	Hardness (HB)	Density (g/cm^3)
Values	157	455	71	150	2.83

Table 4
Johnson-Cook plasticity material constants of aluminium alloy 7075.

Parameters	A (MPa)	B (MPa)	N	C	m
Values	435.701	534.62	0.504	0.970	0.019

Owing to the inaccessibility of acquiring machining power directly from FEA, a basic transformation formula is used to obtain the result, expressed as Eq. (11).

$$P_{cut} = \frac{W_{cut}}{t} = F_{cut} \cdot v \tag{11}$$

where v_f represents the cutting speed, and F_{cut} represents the cutting

force.

The cutting force mechanism of aluminium alloy 7075 plain milling is expressed in Fig. 5.

From Fig. 5, β is the maximum milling angle, and:

$$\beta = arc\cos\left(\frac{t_d - c_w}{t_d}\right) \tag{12}$$

Besides, L is the working path length per tooth and $L = t_d \cdot \beta$. n is the cutter tooth number. The work done is expressed as Eq. (13).

$$W_{rc} = F_{rc} \cdot n \cdot L \tag{13}$$

where F_{rc} is the resultant cutting force. Taking the x axis as an example, the work done by the cutting tool per revolution is given below:

$$W_x = F_x \cdot \sin\left(\frac{1}{\omega t}\right) \cdot n \cdot t_d \cdot \arccos\left(\frac{t_d - c_w}{t_d}\right) \tag{14}$$

where ω is the angular velocity. The basic cutting power consumed by the tool per step is given as:

$$P_{cut} = \frac{W_x}{t} = F_x \cdot \sin\left(\frac{1}{\omega t}\right) \cdot n \cdot t_d \cdot \arccos\left(\frac{t_d - c_w}{t_d}\right) \cdot \frac{\omega}{2\pi} \tag{15}$$

F_x and F_y are calculated as follows when the feed direction is along the x or y-axis.

$$F_x = F_{rc} \cdot \sin(\omega t) + \mu \cdot F_N \tag{16}$$

$$F_y = F_{rc} \cdot \cos(\omega t) \tag{17}$$

where F_N is the axial force. Therefore, the resultant cutting power consumed per step is given as:

$$P_{rc} = P_{cut} + P_f \tag{18}$$

where P_f denotes the radial friction and is expressed as:

$$P_f = \mu \cdot \left(F_x - F_y \tan(\omega t)\right) \cdot v_f \tag{19}$$

The cutting power considering tool wear is obtained as:

$$P_{cut}{}' = P_{rc} + P_{ac} \tag{20}$$

where P_{ac} denotes the additional cutting power due to tool wear in the flank, which is generated by the frictional force of radial extrusion F_{tw} and tangential force of material deformation F_{zw}. P_{ac} is expressed as (Hou et al., 2014):

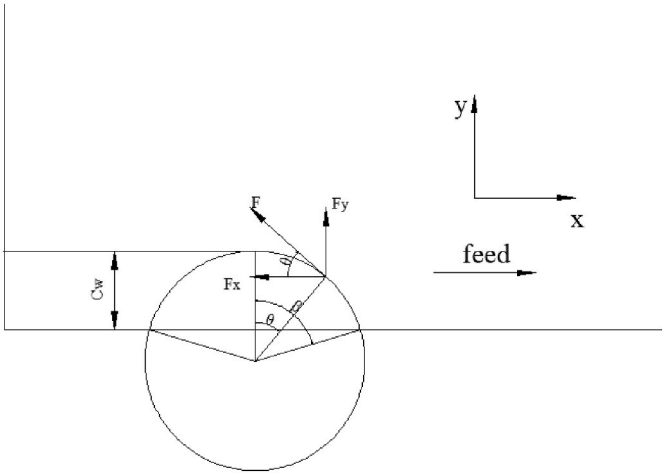

Fig. 5. The cutting force mechanism in plain milling process.

$$P_{ac} = F_{ac} \cdot v' = \begin{bmatrix} F_{tw} \\ F_{zw} \end{bmatrix} \cdot [vf \quad v_r] \tag{21}$$

$$dF_{tw} = \mu \cdot [dF_{zw} + dF_z] \tag{22}$$

$$dF_{zw} = \sigma \cdot \left[vb - \frac{2}{3} vb^*\right] \tag{23}$$

where v_r is the rotary speed of the cutting tool, vb^* is a fixed length of elastic contact area, vb is the flank tool wear obtained according to Usui's model (Zhu and Zhang, 2019).

$$vb = A_c \cdot \sigma_n \cdot v_s \cdot e^{\frac{-B_c}{T_{int}}} \cdot \Delta t \tag{24}$$

where σ_n is the normal pressure, v_s is the sliding speed, T_{int} is the interface temperature, A_c and B_c are constants.

Due to assumptions and simplifications, the FEA based power model in Eq. (20) may have many uncertainties leading to infeasible data for transfer learning. So, it is desirable to quantify the uncertainties as expressed by Eq. (25) and Eq. (26).

$$P_{rc}^{calib} = \alpha_x \cdot \frac{F_x \cdot n \cdot t_d \cdot \omega}{2\pi} \cdot \sin\left(\frac{1}{\omega t}\right) \cdot \arccos\left(\frac{t_d - c_w}{t_d}\right) + \mu \cdot \left(\alpha_x \cdot F_x - \alpha_y \cdot F_y \cdot \tan(\omega t)\right) \cdot v_f \tag{25}$$

$$P \to P^{calib} = P_{rc}^{calib} + P_{ac} + \Delta e \tag{26}$$

From Eq. (25) and Eq. (26), the unknown coefficients include α_x, α_y, Δe. F_z do not need to be calibrated as there is no work in the Z direction in plain milling. Meanwhile, the reason for P_{ac} is that it is calibrated by adding coefficients A_c and B_c. Δe represents errors between observation and simulation.

The calibration indeed borrows the principle of Bayesian parameter estimation (Moreland et al., 2020). Specifically, the Bayesian attempts to obtain the posterior distribution of $\alpha_x, \alpha_y, \Delta e$ by expressing uncertain knowledge as probability statements, making predictions of inference uncertainty possible. The relationship between prior and posterior distribution is given in Eq. (27).

$$f(x|y) = \frac{f(y|x)p(x)}{f(y)} = \frac{f(y|x)p(x)}{\int f(y|x)p(x)dx} \propto f(y|x)p(x) \tag{27}$$

where $p(x)$ and $f(x|y)$ are the prior and posterior distribution of x, $f(y|x)$ is the likelihood function.

To get the solution of $f(y|x)\,p(x)$, the MCMC algorithm is a necessary means (Nemeth and Fearnhead, 2021). It tries to get a stationary distribution by creating a stochastic process on long enough simulation runs. For a chain with Markov property, it has the relationship of $p(x_{i=1}|x_i, x_{i-1}, \cdots, x_1) = p(x_{i+1}|x_i)$. When it converges to the stationary distribution, the posterior distribution of the unknown coefficients is determined.

For sampling, the Gibbs algorithm is used for multi-parameter calibration. Here it is extended to three dimensions to solve the posterior

Table 5
Gibbs sampling algorithm for this study

Gibbs Sampling Algorithm
Input the initial values of $\alpha_x, \alpha_y, \Delta e$
For iteration $i \in (1, n)$**do**
Repeat
$\alpha_x(trail) = p((\alpha_x(i)\|\alpha_y(i), \Delta e(i))$
$\alpha_y(trail) = p((\alpha_y(i)\|\alpha_x(i), \Delta e(i))$
$\Delta e(trail) = p((\Delta e(i)\|\alpha_x(i), \alpha_y(i))$
Until a target Markov chain length is reached
End for
Output $\alpha_x, \alpha_y, \Delta e$

probability densities of $\alpha_x, \alpha_y, \Delta e$. The details are listed in Table 5.

In this paper, the normal distribution serves as the prior distribution of α_x and α_y, while the gamma distribution serves as the prior distribution of Δe, as expressed as Eq. (28) to Eq. (30).

$$\alpha_x \sim N(0,1) \tag{28}$$

$$\alpha_y \sim N(0,1) \tag{29}$$

$$\Delta e \sim Gamma(2,1) \tag{30}$$

The likelihood function of $\alpha_x, \alpha_y, \Delta e$ is defined as:

$$p\left(Y\middle|\theta\right) = \frac{1}{(2\pi\sigma^2)^{N/2}} \exp\left(-\sum_{i=1}^{N}\left[\frac{\left(Y_i^{'} - Y_i\right)^2}{2\sigma^2}\right]\right) \tag{31}$$

The posterior probability density function is expressed as:

$$p\left(\theta\middle|Y\right) = \frac{p(\theta)}{(2\pi\sigma^2)^{N/2}} \exp\left(-\sum_{i=1}^{N}\left[\frac{\left(Y_i^{'} - Y_i\right)^2}{2\sigma^2}\right]\right) \tag{32}$$

where $p(\theta)$ is the prior distribution of $\alpha_x, \alpha_y, \Delta e$; Y_i is the actual value of the ith observed sample, and $Y_i^{'}$ is the theoretical value of the ith observed sample.

3.1.3. Experimental dataset construction

Orthogonal experimental design (OED) (Wang et al., 2020b) is introduced for constructing the experiment dataset. The OED is based on the orthogonality to select some representative points to replace the comprehensive test to make the experiment more efficient. Given the inputs and outputs, an L_{32} (4^9) orthogonal array is formed that could accommodate four levels per feature, where recommendations, machine capacity and experience determine the value per level.

3.2. Learning algorithm

RFR algorithm is adopted as a base learner for TR to train the model. It is an ensemble-learning algorithm that combines a large set of regression trees. The prediction result is obtained by averaging the prediction results of all internal binary decision trees. Compared with other machine learning (e.g., support vector machine), RFR has fewer parameters to be tuned. Moreover, it has shown accuracy comparable with that of a deep learning algorithm, especially for a small sample size, as it is not sensitive to noise or over-fitting. Therefore, RFR is utilised as a base learner to study the nonlinear relationship between the inputs and outputs. The specific information on RFR is found in Li et al. (2020a).

4. Case study

In this section, the proposed approach is validated on python 3.6, and the processor is selected as Intel (R) Core (TM) i5-9400 CPU @ 2.90 GHz and 8 GB RAM.

4.1. Systematic methodology illustration

The systematic methodologies adopted in the case study consist of (1) data acquisition and analysis, (2) model training and application, and (3) performance evaluation, as shown in Table 6.

From Table 6, the methodologies adopted in each step are explained, and the details are presented in the next section.

4.2. Data acquisition and analysis

4.2.1. Data acquisition from simulation

A plain milling simulation for aluminium alloy 7075 parts is conducted, where the tool path in one working step is a rectangle with a diameter of 204 × 37 mm, and the cutting tools are made up of tungsten steel. The milling simulation is carried out in ABAQUS 6.14, as shown in Fig. 6. After simulation, data extraction is performed. Based on the extraction range of input features in Table 7, samples are chosen by LHS with groups of 200. Partial results are listed in Table 8. Besides, the low-pass filter frequency adopted is 12,000, as the lower bound of n is 1500 (r/min).

Taking some features as examples, the three-dimensional distribution of samples acquired from LHS are shown in Fig. 7.

Fig. 7 clearly shows that LHS guarantees good space-filling and uniformity of sampling points along each dimension, ensuring data representativeness for the training process.

Table 6
Systematic methodology explanations.

Procedures	Contents
Step 1: Data collection and analysis	• 32 and 16 groups of actual data collection by OED respectively and data analysis by Sf1001 software where power data is collected under the cutting states. The average value is taken as a measurement result per group and repeated each group five times. Combined with the average time read from the machine tool, the cutting energy consumption is obtained; • 200 groups of simulation data collection by the LHS method. After collection, a low-pass filter is used to filter the simulated signal. The filtering frequency of the low-pass filter is 8 × n, and n is spindle speed. Then, the polynomial fit is used to obtain the filtered signal curve, and the average value is taken from the wave peak. Finally, Bayesian-MCMC calibration is performed with 16 groups of actual data.
Step 2: Model training and application	• Model training by TR-RFR based on a calibrated dataset; • Prediction application analysis in cutting energy consumption of aero-parts.
Step 3: Performance evaluation	• Illustration of target dataset allocation; • Comparison analysis with TR-RFR and RFR using relative errors and other three indicators of root mean squared error (RMSE), coefficient of determination (R^2) and mean absolute error (MAE); • Sensitive analysis by Mean Decrease Gini and Mean Decrease accuracy;

4.2.2. Data acquisition from experiment

An aero part made of aluminium alloy 7075 (chemical composition/wt.%—Al:90.01 Zn:5.43 Si: 0.07 Fe: 0.28 Cu: 1.53 Mn: 0.04 Mg: 2.49 Cr: 0.19 Zn: 5.1–6.1 Ti: 0.03) is selected. The machining process is conducted on Da Lian lathe VDL850A. Cutting power meter PW3360-30 and clamp current sensor 9660 are utilised for measuring cutting power generated per test. Sf1001 data analysis software is used for data analysis. All cutting tests are performed under dry cutting conditions in the context of sustainable manufacturing practices. The experimental setup and data analysis are shown in Fig. 8. The tool path of the workpiece milling is shown in Fig. 9.

To make the experimental data more accurate and reliable, per test is performed five times, so the power value is averaged. The details of levels are shown in Table 9. The experiment design and values with two decimal places are listed in Table 10.

4.2.3. Feasibility evaluation of FEA model and calibration

FEA makes sense if and only if the simulated result proves the good performance. Therefore, the FEA model should be validated to be the cornerstone of transfer learning. In this regard, 16 groups of experimental data are designed for feasibility evaluation and calibration of the FEA model, and the errors between FEA and experimental results are shown in Table 11.

From Table 11, the relative errors are lower than 13%, while the maximum relative error appearing at the 6th experiment is 12.46%. Such errors may be attributed to the fact that it is hard to make accurate

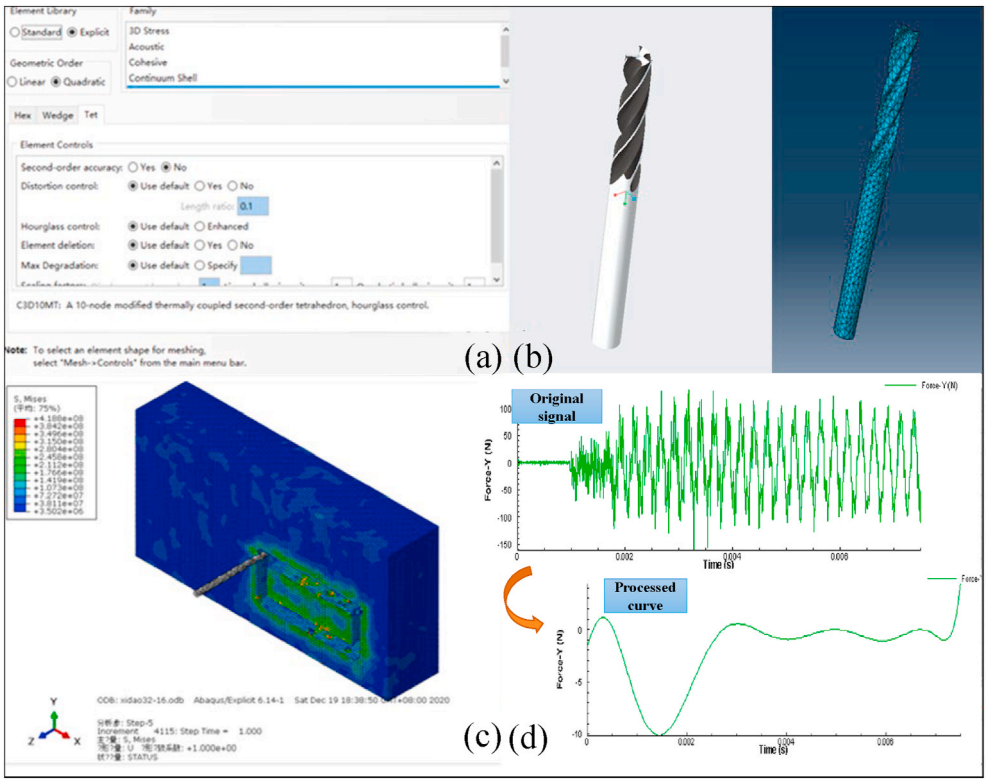

Fig. 6. FEA showing (a) workpiece setup, (b) tool setup, (c) simulation of the milling process and, (d) processed simulation curve of the cutting force taking Y-axis as an example.

Table 7
Sampling range of input features for FEA.

Input feature	c_d (mm)	c_w (mm)	n (r/min)	f_r (mm/r)	t_h (°)	t_{ra} (°)	t_{re} (°)	t_d (mm)
Sampling range	[0.5,2]	[0.5,2]	[1500,3000]	[0.1,0.25]	[20,50]	[10,20]	[10,18]	[4,10]

Table 8
Simulation results.

Exp.no	c_d (mm)	c_w (mm)	n (r/min)	f_r (mm/r)	t_h (°)	t_{ra} (°)	t_{re} (°)	t_d (mm)	Cutting power(w)
1	1.55	0.98	1907	0.13	39	13	12	8	30.75
2	1.37	0.77	2581	0.13	34	17	12	5	19.04
3	1.02	1.30	1573	0.14	36	16	12	7	22.26
…	…	…	…	…	…	…	…	…	…
61	0.61	1.20	2324	0.17	34	15	12	7	16.96
62	1.51	1.40	2347	0.11	43	19	11	10	45.66
63	1.27	1.50	2383	0.16	44	19	10	7	47.87
…	…	…	…	…	…	…	…	…	…
198	1.32	0.70	2246	0.10	36	18	13	8	18.43
199	0.65	1.30	1622	0.15	33	13	12	6	13.69
200	1.46	2.0	1951	0.18	36	16	12	7	53.21

object boundary conditions and material parameters. The uncertainties behind the FEA model remain to be recognised. Therefore, calibration is one necessary work to improve the accuracy of the FEA power model.

As discussed in Section 3.1.2, the Bayesian-MCMC is used to acknowledge the unknown coefficients based on the experiment data, and the posterior results are probability distributions. To make the sampling more stable, the Gibbs method is calculated 1000 times. The iteration is drawn in Fig. 10, and the probability distributions of three unknown calibration coefficients are plotted in Fig. 11. For stability of results, the values of the first 200 iterations are eliminated.

From Figs. 10 and 11, the results are derived from the median of the probability distributions, 0.8729, 1.4533, and 2.3751, with four decimal places, as adopted to calibrate Eq. (26). Thus, the cutting power results of the 200 groups are changed and used for training by TR-RFR in the next section.

4.3. Model training and application

4.3.1. Model training

In this section, model training is exemplified. 32 groups of data in Table 10 are selected as target samples, while 200 groups of calibrated simulation data are viewed as source samples to enable the training process. Meanwhile, the k-fold cross-validation is adopted, which usually guarantees the credibility of testing results and prevents model

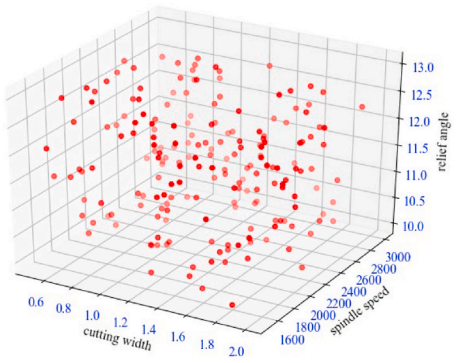

(a) Sample feature distribution of c_w, n and t_{re}

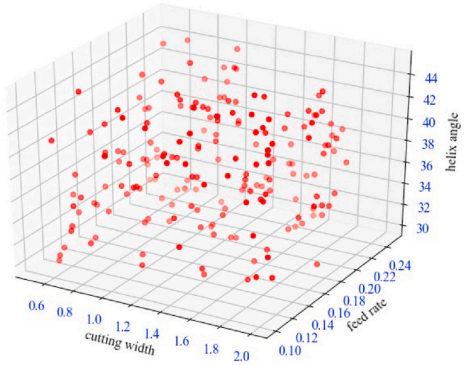

(b) Sample feature distribution of c_w, f_r and t_h

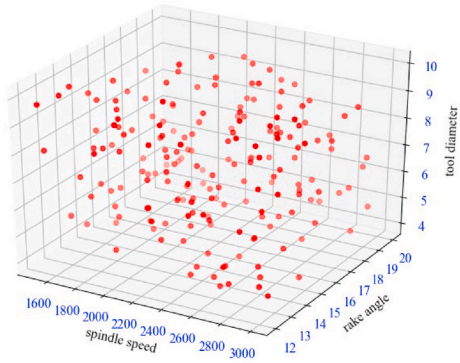

(c) Sample feature distribution of n, t_{ra} and t_d

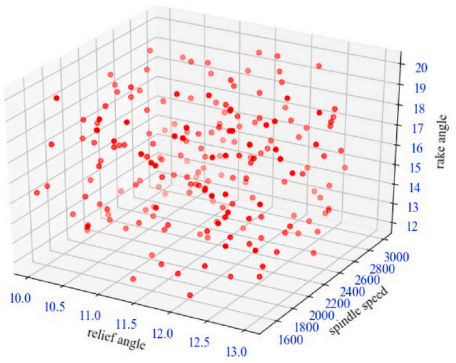

(d) Sample feature distribution of t_{re}, n and t_{ra}

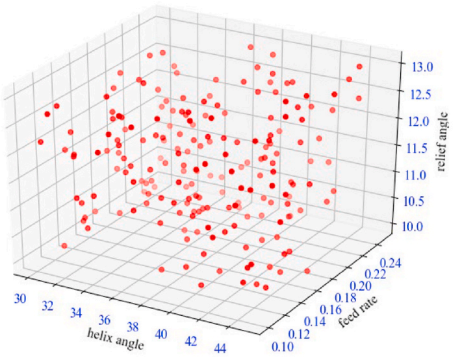

(e) Sample feature distribution of t_h, f_r and t_{re}

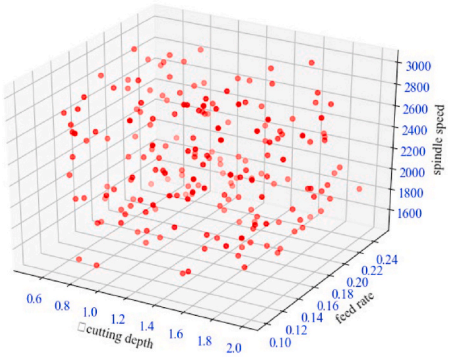

(f) Sample feature distribution of c_d, f_r and n

Fig. 7. Three-dimensional distribution of features.

Fig. 8. The environment setup of the milling process.

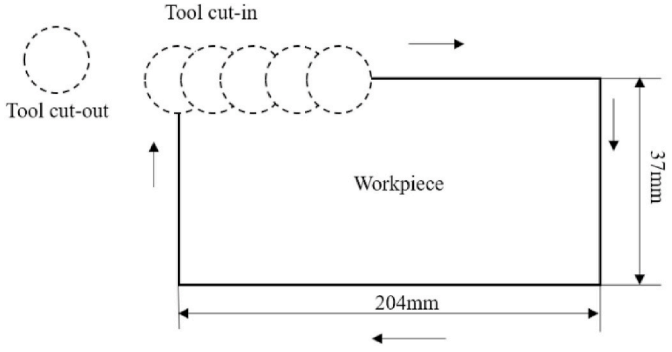

Fig. 9. Workpiece size and tool path.

Table 9
Input features and their levels.

Input feature	c_d (mm)	c_w (mm)	n (r/min)	f_r (mm/r)	t_h (°)	t_{ra} (°)	t_{re} (°)	t_d (mm)
Level 1	0.5	0.5	1500	0.1	30	12	10	4
Level 2	1	1	2000	0.15	35	14	11	6
Level 3	1.5	1.5	2500	0.2	40	16	12	8
Level 4	2	2	3000	0.25	45	20	13	10

overfitting, especially suitable to the small experiment samples. K is set as 4, meaning 3 folds of the target data are used for training, and 1-fold is left aside to support model testing. And testing is repeated 4 rounds. Furthermore, the number of trees is set as 300, the maximum depth of the trees is 50, the minimum number of samples at a leaf node is 5, and the minimum splitting feature is 3.

4.3.2. Prediction application

The cutting energy consumption prediction of the parts milling process is performed. As mentioned in Section 2.1, one important parameter needs to be predetermined, i.e., the time expensed in the cutting state:

$$t_{cut} = \frac{L}{v_f} \tag{33}$$

$$v_f = n \cdot f_r \tag{34}$$

where L is the cutting path, v_f is cutting speed mm/min. As L is a square straight path in this study, the time is expressed as Eq. (35).

$$t_{cut} = 2 \cdot \frac{(L_w + L_l - 2 \cdot c_w + t_d)}{v_f} \tag{35}$$

Therefore, cutting energy consumption is listed in Table 12. Compare the results with the actual value of the time read from the machine and take an average of five times. Meanwhile, the average prediction time of 32 experiments is 17.7 ms.

From Table 12, it is found that the relative errors are basically lower than 10%, and the average errors of the four rounds are 3.99%, 6.24%, 6.56% and 4.63%, respectively, proving the excellent performance of the proposed method. Although larger error fluctuation remains, such as 3rd in round 2 with 9.86%, it does not mean infeasibility of the proposed methods, given that the real world is neither detailed nor accurate and operations like round-off are generally unavoidable. In conclusion, the results show that the proposed method reaches good accuracy in predicting cutting energy consumption for aviation parts. The results also remind us of the importance of a good dataset supplement where model prediction accuracy is affected by an expensive data-labelling environment.

Table 10
Experiment design and the values.

Exp.no	c_d (mm)	c_w (mm)	n (r/min)	f_r (mm/r)	t_h (°)	t_{ra} (°)	t_{re} (°)	t_d (mm)	Cutting power(w)
1	0.50	0.50	1500	0.10	30	12	11	4	12.45
2	0.50	1.00	2000	0.15	35	14	12	6	14.52
3	0.50	1.50	2500	0.20	40	16	13	8	25.66
4	0.50	2.00	3000	0.25	45	20	14	10	44.21
5	1.00	0.50	1500	0.15	35	16	13	10	15.37
6	1.00	1.00	2000	0.10	30	20	14	8	20.65
7	1.00	1.50	2500	0.25	45	12	11	6	48.51
8	1.00	2.00	3000	0.20	40	14	12	4	47.47
9	1.50	0.50	2000	0.20	45	12	12	8	27.30
10	1.50	1.00	1500	0.25	40	14	11	10	51.71
11	1.50	1.50	3000	0.10	35	16	14	4	43.97
12	1.50	2.00	2500	0.15	30	20	13	6	63.32
13	2.00	0.50	2000	0.25	40	16	14	6	36.18
14	2.00	1.00	1500	0.20	45	20	13	4	49.06
15	2.00	1.50	3000	0.15	30	12	12	10	88.56
16	2.00	2.00	2500	0.10	35	14	11	8	71.13
17	0.50	0.50	3000	0.10	45	14	13	6	18.39
18	0.50	1.00	2500	0.15	40	12	14	4	39.21
19	0.50	1.50	2000	0.20	35	20	11	10	25.81
20	0.50	2.00	1500	0.25	30	16	12	8	29.39
21	1.00	0.50	3000	0.15	40	20	11	8	19.00
22	1.00	1.00	2500	0.10	45	16	12	10	24.97
23	1.00	1.50	2000	0.25	30	14	13	4	36.93
24	1.00	2.00	1500	0.20	35	12	14	6	41.71
25	1.50	0.50	2500	0.20	30	14	14	10	33.27
26	1.50	1.00	3000	0.25	35	12	13	8	63.38
27	1.50	1.50	1500	0.10	40	20	12	6	31.39
28	1.50	2.00	2000	0.15	45	16	11	4	47.76
29	2.00	0.50	2500	0.25	35	20	12	4	76.84
30	2.00	1.00	3000	0.20	30	16	11	6	63.12
31	2.00	1.50	1500	0.15	45	14	14	8	73.77
32	2.00	2.00	2000	0.10	40	12	13	10	70.92

Table 11
Samples for feasibility evaluation and calibration.

Exp. no	c_d (mm)	c_w (mm)	n (r/min)	f_r (mm/r)	t_h (°)	t_{ra} (°)	t_{re} (°)	t_d (mm)	experiment Power(w)	Simulation Power(w)	|Relative Error| (%)
1	1.00	1.00	2000	0.20	35	14	12	6	19.62	21.05	7.29
2	1.50	1.00	2000	0.20	30	12	11	8	31.85	34.82	9.32
3	2.00	1.50	3000	0.15	30	20	11	10	58.35	59.63	2.19
4	0.50	1.00	3000	0.25	45	16	12	4	20.19	18.90	6.39
5	1.00	0.50	2500	0.10	35	16	13	6	27.80	29.11	4.71
6	2.00	2.00	3000	0.25	45	18	11	10	65.23	73.36	12.46
7	2.00	0.50	2500	0.25	45	12	12	6	42.80	38.75	9.46
8	1.00	2.00	3000	0.10	40	14	13	4	26.55	28.14	5.99
9	0.50	0.50	2000	0.30	40	12	11	4	30.49	33.87	11.09
10	1.00	1.00	3000	0.25	40	14	13	4	41.73	43.90	5.20
11	0.50	1.00	1500	0.20	35	12	14	8	13.24	12.89	2.64
12	2.00	2.00	3000	0.25	45	14	14	10	77.37	76.31	1.37
13	1.50	1.50	2500	0.25	40	16	13	8	73.72	80.27	8.88
14	2.00	0.50	1500	0.10	35	16	13	8	55.81	60.24	7.94
15	1.50	2.00	1500	0.15	30	14	12	6	32.97	32.45	1.58
16	0.50	2.00	3000	0.20	35	16	11	4	61.64	58.21	5.56

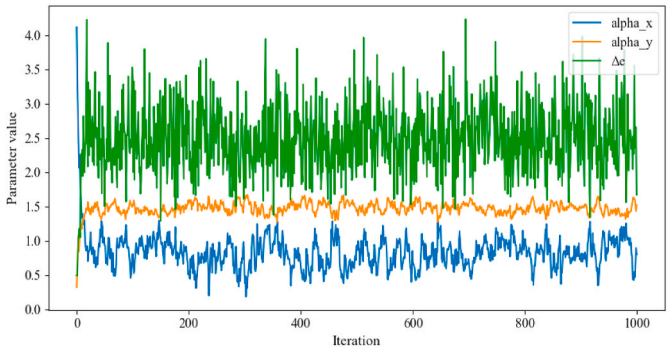

Fig. 10. Iterative process of sampling.

4.4. Performance evaluation and sensitive analysis

4.4.1. Illustration of experiment dataset allocation

In the previous section, 4-fold cross-validation is used to split the training and testing samples of the experiment target data (TD), where 75% of TD involves training in each round. To illustrate the reasonable allocation, four studies are performed:

(1) No_TD, meaning only source data (SD) is used to train the model. The TD only involves testing.
(2) 1/4*TD, meaning 8 groups of experimental data with SD, are used to train the model. The left 24 groups are for testing.
(3) 1/2*TD, representing 16 groups with SD involved in training.
(4) 3/4*TD, representing 24 groups with SD involved in training.

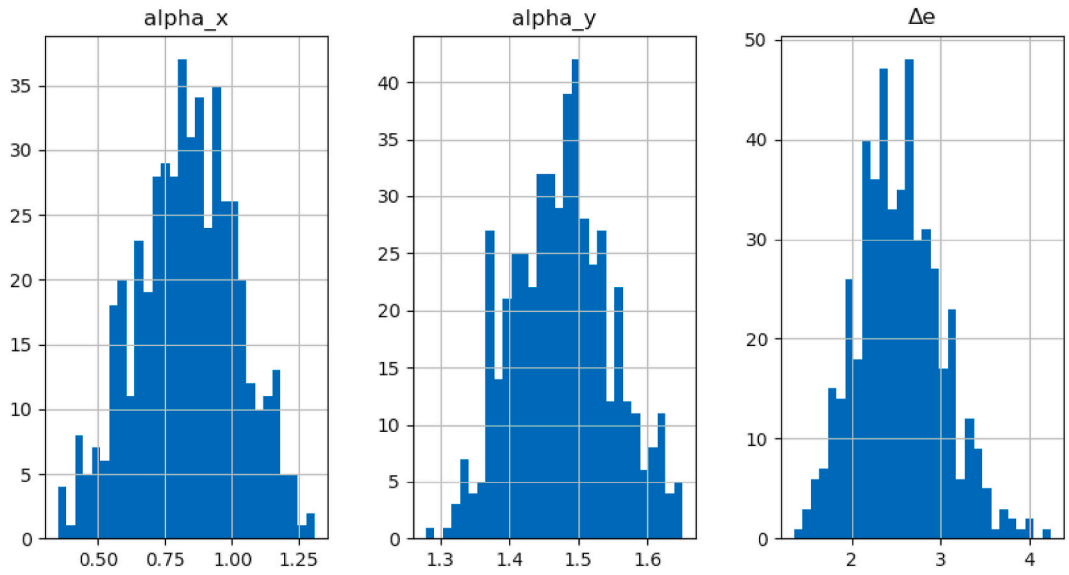

Fig. 11. The probability distributions of three values.

Table 12
Prediction of cutting energy consumption compared with true values.

Samples		Predicted Result (J)	True Result (J)	Predicted Time (s)	True Time (s)	|Relative Error|%
Round 1	1	3861.95	4051.79	97.20	97.14	4.69
	2	6040.31	6213.01	195.20	197.93	2.78
	4	1611.54	1774.93	39.52	40.15	9.21
	4	2108.89	2063.54	133.33	134.26	2.20
	5	2148.88	2183.92	59.04	60.36	1.60
	6	4754.32	4532.62	96.40	94.95	4.89
	7	8878.70	8496.30	117.60	119.45	4.50
	8	2212.66	2258.74	78.40	76.85	2.04
	Avg|Relative Error|%					3.99
Round 2	1	2099.14	2084.11	58.08	56.43	0.72
	2	5577.27	5689.21	66.13	64.24	1.97
	3	2303.61	2555.48	39.52	40.32	9.86
	4	1913.33	2077.25	74.40	76.09	7.89
	5	1936.45	1868.08	74.40	72.38	3.66
	6	11202.49	10373.63	148.20	146.27	7.99
	1	4447.03	4870.00	97.20	99.27	8.69
	8	3909.96	4303.51	96.80	97.87	9.14
	Avg|Relative Error|%					6.24
Round 3	1	1402.16	1510.21	59.04	58.85	7.15
	2	3303.11	3182.80	49.00	50.42	3.78
	3	1985.65	2000.44	60.00	60.13	0.74
	4	9316.48	9847.64	131.20	133.49	5.39
	5	4423.43	4208.96	79.68	81.41	5.10
	3	2971.19	2935.59	119.52	117.56	1.21
	7	2811.22	3034.86	148.20	146.97	7.37
	8	2353.90	2208.91	46.85	45.54	6.56
	Avg|Relative Error|%					4.66
Round 4	1	1324.07	1240.97	66.13	65.31	6.70
	2	2229.71	2441.07	195.2	196.07	8.66
	3	1458.09	1384.90	98.00	95.38	5.29
	6	3851.04	3700.30	46.85	48.16	4.07
	5	3056.06	3009.27	77.76	76.75	1.55
	6	5066.75	4947.10	77.76	78.13	2.42
	7	1955.02	1851.01	98.40	100.65	5.62
	8	2244.88	2307.45	48.20	48.61	2.71
	Avg|Relative Error|%					4.63

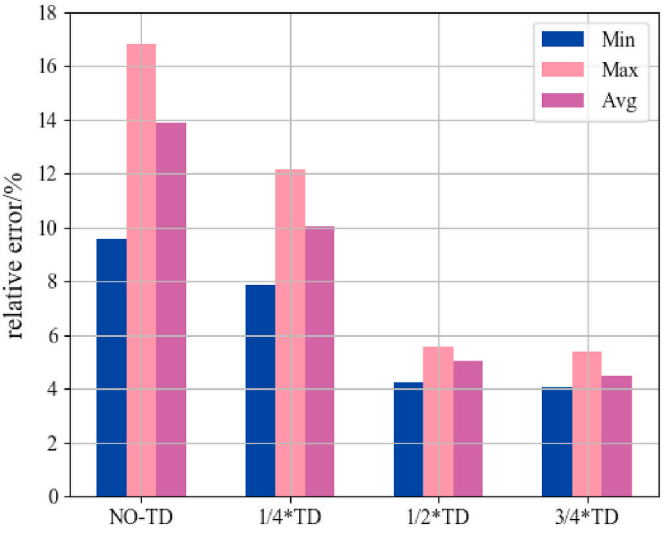

Fig. 12. Numbers of the experimental data used in model training.

Then, the testing average, maximum and minimum relative values of the predicted cutting power are presented in Fig. 12.

From Fig. 12, it is found that with the increase of training numbers of TD, the proposed method is getting better according to the average, maximum and minimum relative errors and is slightly improved from 16 to 24 groups, taking the average relative error as an example. When the numbers increase from 0 to 8 groups (in the case of 'No_TD' and '1/4*TD'), the error drops from 13.90% to 10.03%. A similar observation is seen from the case of '1/4*TD' to '1/2*TD' with a reduction of 4.98%. However, when the numbers increase from 16 to 24 groups, the error decreases from 5.05% to 4.73%. This means that the proposed method is slightly improved (with a reduction of 0.32%) and indicates that the performance starts to converge when the experiment training numbers are around 16 to 24 groups. Thus, the experiment data allocation of this paper is reasonable.

4.4.2. Performance evaluation

In this section, the performance of the proposed method is examined. Two methods used for comparison are outlined below:

Table 13
Average relative errors of the three methods.

Methods	Round 1		Round 2		Round 3		Round 4	
	Training	Testing	Training	Testing	Training	Testing	Training	Testing
RFR	8.99%	9.31%	13.26%	13.41%	13.08%	15.47%	10.87%	12.50%
TR-RFR	6.04%	7.72%	6.81%	8.64%	5.80%	7.39%	7.46%	8.55%
The proposed method	2.45%	3.86%	4.00%	5.38%	3.66%	4.75%	2.93%	4.52%

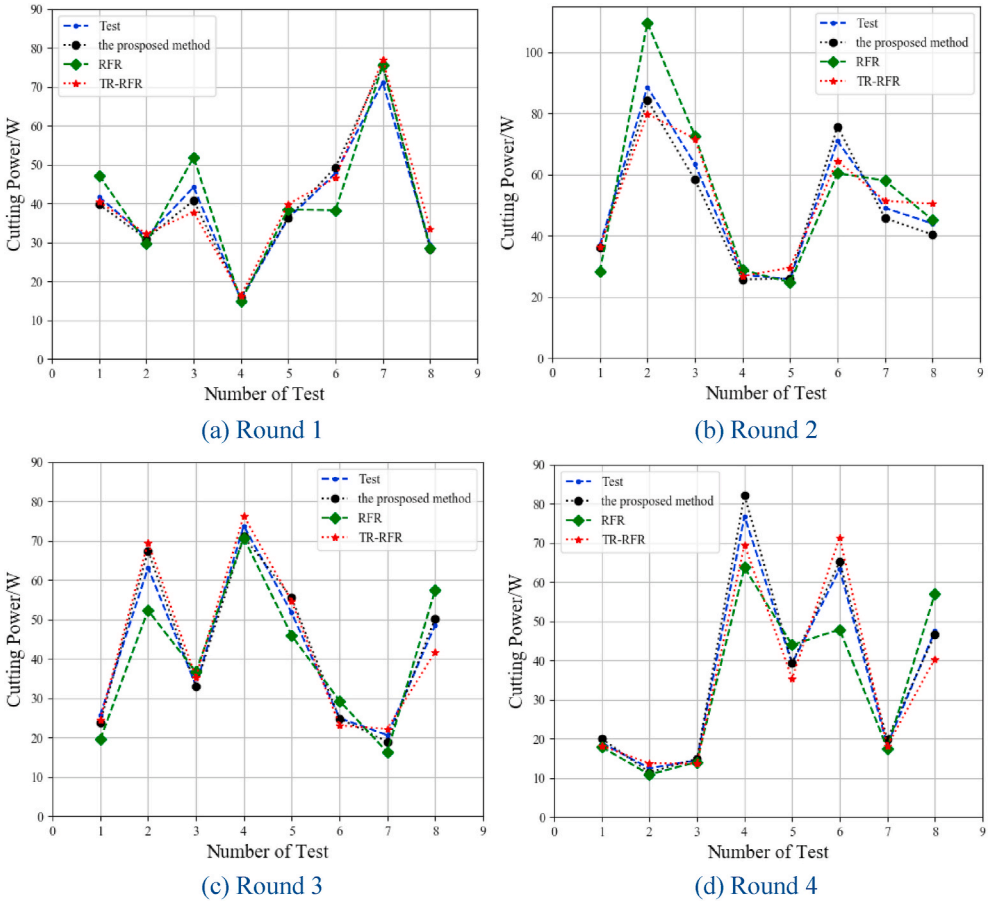

Fig. 13. Fitting curves of the three methods.

Table 14
Comparison testing results of the three methods.

Method	Round 1			Round 2			Round 3			Round 4		
	RMSE	MAE	R^2	RMSE	MAE	R^2	RMSE	MAE	R^2	RMSE	MAE	R^2
RFR	5.097	4.042	0.888	9.979	7.767	0.766	6.386	5.850	0.878	8.114	5.833	0.873
TR-RFR	3.707	3.040	0.940	5.558	4.615	0.927	3.770	3.156	0.957	3.693	4.833	0.955
The proposed method	2.209	1.703	0.979	2.933	3.401	0.972	2.500	2.958	0.981	2.161	1.509	0.991

- RFR: training the model without calibration and transfer operations to see if the two operations have values in prediction accuracy. Training and testing datasets are set as same as the proposed method without the 200 groups of simulation data.
- TF-RFR: training the model without calibration to see if the operation is effective. Training and testing datasets are set as same as the proposed method.

The training and testing average errors of the above three methods are listed in Table 13. The fitting curves of the methods are shown in Fig. 13, taking testing results as examples.

From Table 13, the testing relative errors of the three methods are close to the training errors with a reduction of no more than 2.39%, which verifies the good stability of the methods, indicating that almost no model over-fitting exists with a large difference between the training and testing results (Sarle, 1995). Meanwhile, taking the testing average relative errors as an example, the performance of TR-RFR and the proposed method are far better than RFR, showing that the feasibility of the data supplement from a reliable source domain. More than this, the proposed method with the lower average relative errors of 3.86%, 5.38%, 4.75%, and 4.52% than TR-RFR with 7.72%, 8.64%, 7.39% and 8.55%, suggesting that calibration of the source data is one way to

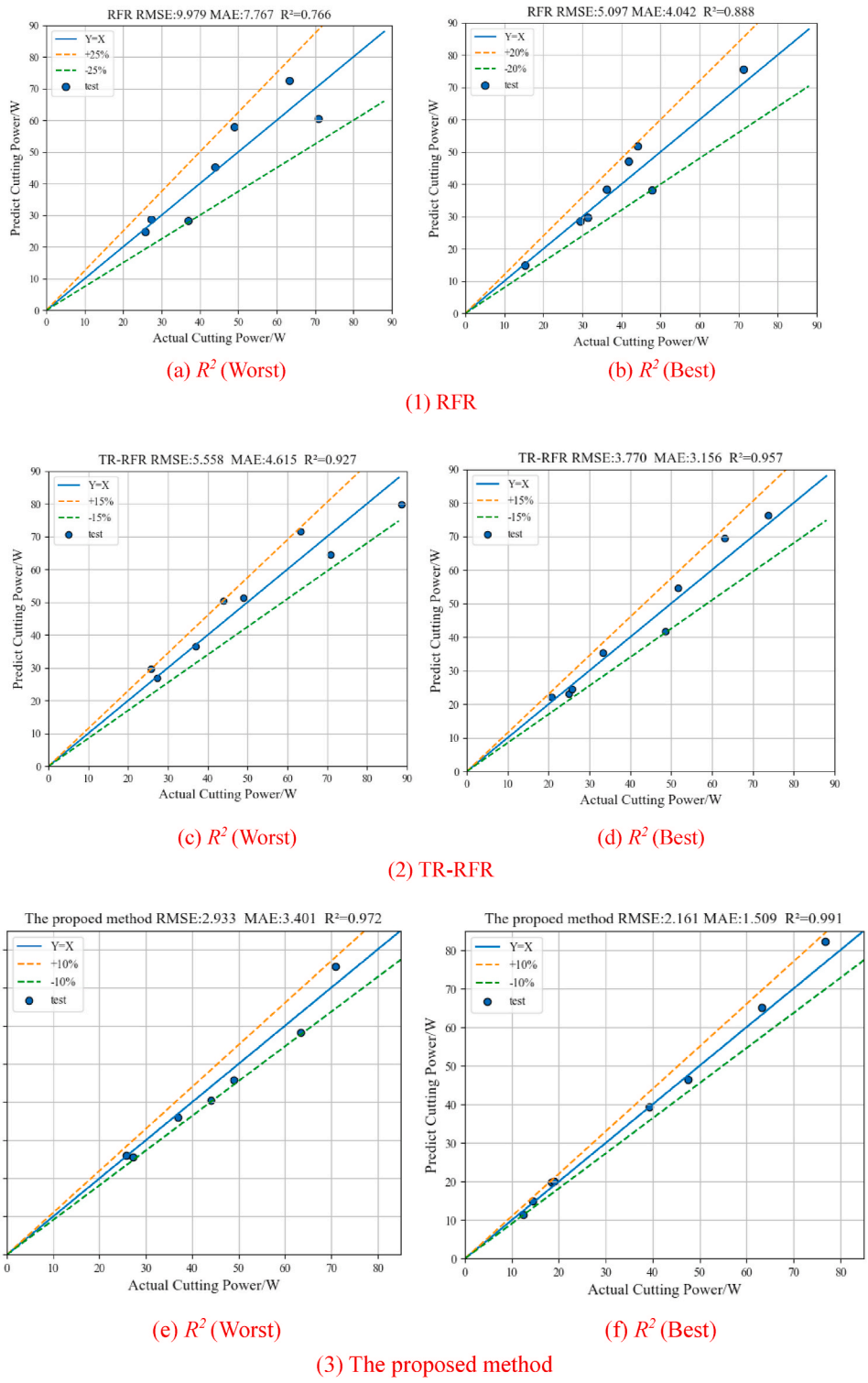

Fig. 14. Error values of the three methods.

improve the prediction model's reliability further.

This conclusion is observed directly in Fig. 13. The proposed methods could fit the actual responses curve well, followed by TR-RFR and RFR algorithms. This happens because there are enough reliable data for training, so the proposed method studies the complex nonlinear relationship between the inputs and output well.

To demonstrate the superiority of the method further, *RMSE*, R^2 and *MAE* are introduced, and the comparison results are shown in Table 14. Among them, *RMSE* measures the residual variances between predicted and observed values, *MAE* reflects the average errors, whereas R^2 reflects the fitness of the regression line to observed values. Meanwhile, as R^2 could describe the global goodness of fit of the prediction method without dimensions interference (Parhizkar et al., 2021), it is taken as an example. The worst and best R^2 curves of the three methods are found in Fig. 14.

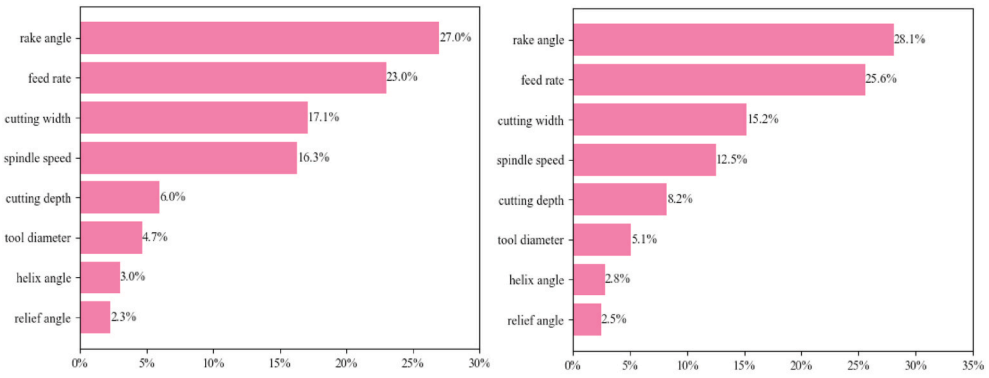

(a) Mean Decrease Gini (b) Mean Decrease accuracy

Fig. 15. Importance weight of each feature.

$$RMSE = \sqrt{\frac{\sum_{i=1}^{n}(y_i - \hat{y}_i)}{n}} \tag{36}$$

$$R^2 = 1 - \frac{\sum_{i=1}^{n}(y_i - \hat{y}_i)^2}{\sum_{i=1}^{n}(y_i - \dot{y}_i)^2} \tag{37}$$

$$MAE = \frac{1}{n}\sum_{i=1}^{n}|\hat{y}_i - y_i| \tag{38}$$

where $\hat{y}_i$ represents the predicted values, $\dot{y}_i$ represents the mean of response variables, n represents the number of observations. The closer the values of *RMSE* and *MAE* are to 0, the better the quality is. Conversely, the closer of the R^2 value is to 1, the better the performance is.

From Table 14, the *RMSE*, R^2 and *MAE* values of the proposed method outperform the other two algorithms, and RFR performs worst according to the indicators of the four groups. More than this, the three indicators of TR-RFR relative to that of RFR are improved by transfer learning operation, and the proposed method is better performed than TR-RFR thanks to calibration operation. In terms of the accuracy improvement, R^2 is selected as a representative metric. Results show that the proposed method has the best R^2 improved by 11.60% and 3.55% relative to RFR and TR-RFR. It can be attributed to the fact: on the one hand, the valid knowledge of simulation is supplemented, improving the poor prediction capacity due to expensive experiment data extraction; on the other hand, the knowledge of the experiment offers the potentials to calibrate the FEA mechanism model.

Similar conclusions are made in Fig. 14. Although apparent deviations exist in the final point of the worst and best R^2 curves, the overall performance is relatively remarkable, proving good consistency of the proposed prediction method.

4.4.3. Sensitive analysis

To reveal the contributions of the inputs to cutting energy consumption, sensitivity analysis is performed by built-in programs of RFR, i.e., Mean Decrease Gini and Mean Decrease accuracy, two effective ways to reveal important features (Li et al., 2020b). Among them, the importance of the latter is evaluated by average decrements of Mean Square Error. The results are normalised and transformed to importance weights with one decimal place by Eq. (39), as presented in Fig. 15.

$$w_i = \frac{|g_i|}{\sum_{i=1}^{8}|g_i|} \tag{39}$$

where g_i denotes the importance of i_{th} feature. The greater the g_i, the greater the influence of the feature i on the prediction results.

From Fig. 15, it is concluded that the factor mainly influences cutting energy consumption in the case is topped by rake angle (27.0% and 28.1%), followed by feed rate, cutting width and spindle speed. It indicates that the cutting parameters and tool geometries should be judged jointly to get high accuracy of tool wear-related cutting energy. Meanwhile, it gives the future optimisation focus.

4.5. Discussion

In this section, a triangulation methodology is adopted to illustrate the effectiveness of the proposed method. To begin with, taking R^2 in Table 14 as an example, a comparative analysis with other existing works, i.e., the data-driven methods (e.g., RFR) and the transfer learning methods (e.g., TR-RFR), is performed, then each result is drawn. After that, the contributions of the proposed method related to the results are highlighted.

The proposed method is first compared with RFR, a widely used method in parts cutting energy or force prediction (Charalampous, 2021). From Table 14, the worst (0.972) and best R^2 values (0.991) of the proposed method are better than RFR (0.762 and 0.888), showing that the former could capture complex correlations more effectively than the latter with the same small experiment samples. It also indicates that the traditional data-driven methods exceptionally rely on actual rich samples. This observation is confirmed by the related literature that uses such methods. For example, in the study of Azmi (2015) that uses the adaptive neural fuzzy inference system and the study of Xu et al. (2020) that uses ANN, large amounts of actual data are in great need (e.g., 231 and 186 experiment datasets are used in the two works). Obviously, those methods challenge their applications in the aero-machining sector that are featured by expensive data collection. Unlike the existing data-driven methods, by utilising a transferring operation, the proposed method makes the prediction for aviation parts feasible, avoiding the costly collection of experiment data.

Compared with TR-RFR (with the worst value 0.927 and best value 0.957), the proposed method also performs better. The superiority over the traditional transfer learning method lies in its ability in reducing the negative transfer impacts from a similar source on the prediction accuracy by adopting the Bayesian-MCMC calibration. In addition to the TR-RFR, another advanced method used in the existing literature is an ANN-based transfer learning in Wang et al. (2021), where a model concerning cutting force was trained by a transfer network with simulation and experimental data. However, the model's performance still relies on large amounts of experiment data (300 groups). More than this, the author neglects the uncertainties of simulation that may have negative transfer effects, thus limiting the accuracy. By contrast, a conclusion is demonstrated that the proposed method with the calibration is the first one that allows predicting with small amounts of actual data and offers the simulation more feasible in real applications.

Based on the above comparative analysis, it is shown that the proposed method can obtain better performance by solving the drawbacks of the methods in the existing literature, namely its main contributions include: 1) First, unlike the existing data-driven methods, it breaks the limitations of the costly experimental data-labelling through transferring valid knowledge from a similar source domain; 2) Second, unlike the existing transfer learning methods, it considers the negative transfer impacts by using the Bayesian-MCMC calibration to mitigate the uncertainties of the source domain. The ensemble approach holds for any mechanical machining process of parts, provided that the process can be simulated to obtain data. And it is more suitable for the aviation scenario featured by the costly data-labelling. With the desirable accuracy of the proposed method, managers can use energy-saving optimisation to determine the most efficient process plans without numerous experimental trials, avoiding wastes of time, materials, energy, and workforces, which significantly contributes to green manufacturing. As a result, it benefits the industry and society.

5. Conclusions

This paper proposes an ensemble transfer learning approach for aero parts cutting energy consumption prediction, suitable for the non-sustainable expensive-data acquisition and tool wear-existence environment. The main theoretical contributions are summarised as follows.

Firstly, given the machining feature of aero-parts, a data-driven training model is formulated where parameters of cutting and tool conditions affecting tool wear are selected as inputs to make the prediction practical.

Secondly, two main operations are performed orderly, aiming at the problems of limited data available and the high cost of acquiring test data. One is the Bayesian-MCMC calibration for describing the uncertainty of the FEA model to reduce the noise of supplemented data. The other is the TR-RFR for identifying and transferring useful calibrated FEA data to supplement training data.

Finally, the case study has shown that the proposed method performs well in cutting energy consumption prediction with small amounts of actual data. Compared with RFR and TR-RFR, the accuracy is improved by adding transfer learning and calibration operation. Taking R^2 as an example, the best value of the proposed method is increased by 11.60% and 3.55% with the above operations, illustrating the effectiveness.

The main practical implications are as follow. First, its powerful approximation ability in the actual case without repeatedly experiments via a sustainable and reliable way to obtain data and adaptability to different inputs values makes it convenient for the industry to evaluate the cutting energy consumption degree under various process plans. Second, its decisive role in revealing sensitive parameters and helping to formulate energy-saving process settings, beneficial for society, industry and government managers to promote sustainable schemes for aerospace manufacturing.

Potential limitations and related future studies of the paper are as follows. Firstly, the element birth and death method can be used to speed up the simulation process in future studies. Secondly, the proposed method has not yet been applied to complex aero-part like impellers, which will be investigated in the future to fit the prediction model in reality. Finally, cutting energy will be minimised in the future through cutting parameters and tool geometries optimisation according to sensitive analysis results to explore the energy conservation potential of the actual industry.

CRediT authorship contribution statement

Fengyi Lu: Writing – original draft, Methodology, Conceptualization. **Guanghui Zhou:** Supervision, Validation, Writing – review & editing, Project administration, Funding acquisition. **Yang Liu:** Supervision, Validation, Writing – review & editing. **Chao Zhang:** Writing – review & editing.

Declaration of competing interest

The authors declare that they have no known competing financial interests or personal relationships that could have appeared to influence the work reported in this paper.

Acknowledgements

This work was supported by the National Natural Science Foundation of China (Grant No. 51975463) and FlexSUS: Flexibility for Smart Urban Energy Systems (Project No. 91352), which has received funding in the framework of the joint programming initiative ERA-Net Smart Energy Systems' focus initiative Integrated, Regional Energy Systems, with support from the European Union's Horizon 2020 research and innovation programme under grant agreement No. 775970. The usual disclaimer applies.

References

Ali, Khan M., Jaffery, S.H.I., Khan, M., Younas, M., Butt, S.I., Ahmad, R., Warsi, S.S., 2019. Statistical analysis of energy consumption, tool wear and surface roughness in machining of Titanium alloy (Ti-6Al-4V) under dry, wet and cryogenic conditions. Mech. Solid. 10, 561–573.

Arafat, M., Sjafrizal, T., Anugraha, R.A., 2020. An artificial neural network approach to predict energy consumption and surface roughness of a natural material. SN. Appl. Sci. 2, 1–11.

Azmi, A.I., 2015. Monitoring of tool wear using measured machining forces and neuro-fuzzy modelling approaches during machining of GFRP composites. Adv. Eng. Software 82, 53–64.

Bolar, G., Das, A., Joshi, S.N., 2018. Measurement and analysis of cutting force and product surface quality during end-milling of thin-wall components. Measurement 121, 190–204.

Charalampous, P., 2021. Prediction of cutting forces in milling using machine learning algorithms and finite element analysis. J. Mater. Eng. Perform. 30, 2002–2013.

Chen, F., Qu, H., Wu, W., Zheng, J., Qu, S., Zheng, Y.H., 2021. A physical-based plane stress constitutive model for high strength AA7075 under hot forming conditions. Metals-Basel. 11, 314.

Chen, Y., Shen, L., Li, R., Xu, X., Hong, H., Lin, H., Chen, J., 2020. Quantification of interfacial energies associated with membrane fouling in a membrane bioreactor by using BP and GRNN artificial neural networks. J. Colloid. Interf. SCI. 565, 1–10.

Dahbi, S., Ezzine, L., EL Moussami, H., 2017. Modeling of cutting performances in turning process using artificial neural networks. Int. J. Eng. Bus. Manag. 9 https://doi.org/10.1177/1847979017718988.

Dai, W., Yang, Q., Xue, G., Yu, Y., 2007. Boosting for transfer learning. In: Proceedings of the 24th International Conference on Machine Learning, pp. 193–200. https://doi.org/10.1145/1273496.1273521.

Deng, Y., Zhou, X., Shen, J., Xiao, G., Hong, H., Lin, H., Wu, F., Liao, B., 2021. New methods based on back propagation (BP) and radial basis function (RBF) artificial neural networks (ANNs) for predicting the occurrence of haloketones in tap water. Sci. Total Environ. 772, 145534.

Deng, Z., Zhang, H., Fu, Y., Wan, L., Liu, W., 2017. Optimisation of process parameters for minimum energy consumption based on cutting specific energy consumption. J. Clean. Prod. 166, 1407–1414.

Gialos, A.A., Zeimpekis, V., Alexopoulos, N.D., Kashaev, N., Riekehr, S., Karanika, A., 2018. Investigating the impact of sustainability in the production of aeronautical subscale components. J. Cean. Prod. 176, 785–799.

He, Y., Wu, P., Li, Y., Wang, Y., Tao, F., Wang, Y., 2020. A generic energy prediction model of machine tools using deep learning algorithms. Appl. Energy 275, 115402.

Hong, H., Zhang, Z., Guo, A., Shen, L., Sun, H., Liang, Y., Wu, F., Lin, H., 2020. Radial basis function artificial neural network (RBF ANN) as well as the hybrid method of RBF ANN and grey relational analysis able to well predict trihalomethanes levels in tap water. J. Hydrol. 591, 125574.

Hou, Y., Zhang, D., Wu, B., Luo, M., 2014. Milling force modeling of worn tool and tool flank wear recognition in end milling. IEEE ASME Trans. Mechatron. 20, 1024–1035.

Hu, L., Liu, Y., Lohse, N., Tang, R., Lv, J., Peng, C., Evans, S., 2017a. Sequencing the features to minimise the non-cutting energy consumption in machining considering the change of spindle rotation speed. Energy 139, 935–946.

Hu, L., Peng, C., Evans, S., Peng, T., Liu, Y., Tang, R., Tiwari, A., 2017b. Minimising the machining energy consumption of a machine tool by sequencing the features of a part. Energy 121, 292–305.

Kaczyński, P., Skwarski, M., Jaśkiewicz, K., 2020. Development of the technology for press-forming of energy-absorbing elements made of 7075 aluminum alloy. J. Manuf. Process. 50, 676–683.

Khan, A.M., Gupta, M.K., Hegab, H., Jamil, M., Mia, M., He, N., Song, Q., Liu, Z., Pruncu, C.I., 2020. Energy-based cost integrated modelling and sustainability assessment of Al-GnP hybrid nanofluid assisted turning of AISI52100 steel. J. Clean. Prod. 257, 120502.

Li, J., Tian, Y., Zhu, Y., Zhou, T., Li, J., Ding, K., Li, J., 2020a. A multicenter random forest model for effective prognosis prediction in collaborative clinical research network. Artif. Intell. Med. 103, 101814.

Li, L., Chen, S., Yang, C., Meng, F., Sigrimis, N., 2020b. Prediction of plant transpiration from environmental parameters and relative leaf area index using the random forest regression algorithm. J. Clean. Prod. 261, 121136.
Li, Y., Zou, C., Berecibar, M., Nanini-Maury, E., Chan, J.C., Van den Bossche, P., Van Mierlo, J., Omar, N., 2018. Random forest regression for online capacity estimation of lithium-ion batteries. Appl. Energy 232, 197–210.
Lin, H., Dai, Q., Zheng, L., Hong, H., Deng, W., Wu, F., 2020. Radial basis function artificial neural network able to accurately predict disinfection by-product levels in tap water: taking haloacetic acids as a case study. Chemosphere 248, 125999.
Liu, H.Z., Zong, W.J., 2019. Prediction model of tool wear volume in precision turning of ceramic particle reinforced aluminum matrix composites. J. Adv. Manuf. Technol. 100, 2689–2700.
Luo, H., Fu, J., Wu, T., Chen, N., Li, H., 2021. Numerical simulation and experimental study on the drilling process of 7075-t6 aerospace aluminum alloy. Metarials 14, 553.
Lv, L., Deng, Z., Meng, H., Liu, T., Wan, L., 2020. A multi-objective decision-making method for machining process plan and an application. J. Clean. Prod. 260, 121072.
Lv, M., Li, Y., Chen, L., Chen, T., 2019. Air quality estimation by exploiting terrain features and multi-view transfer semi-supervised regression. Inf. Sci. 483, 82–95.
Moreland, J.S., Bernhard, J.E., Bass, S.A., 2020. Bayesian calibration of a hybrid nuclear collision model using p– Pb and Pb-Pb data at energies available at the CERN Large Hadron Collider. Phys. Rev. C 101, 024911.
Nemeth, C., Fearnhead, P., 2021. Stochastic gradient Markov chain Monte Carlo. J. Am. Stat. Assoc. 1–18.
Niu, S., Hu, Y., Wang, J., Liu, Y., Song, H., 2020. Feature-based distant domain transfer learning. In: 2020 IEEE International Conference on Big Data (Big Data), pp. 5164–5171. https://doi.org/10.1109/BigData50022.2020.9378493.
Parhizkar, T., Rafieipour, E., Parhizkar, A., 2021. Evaluation and improvement of energy consumption prediction models using principal component analysis based feature reduction. J. Clean. Prod. 279, 123866.
Pereira, R.B.D., Leite, R.R., Alvim, A.C., de Paiva, A.P., Ferreira, J.R., Davim, J.P., 2017. Multi-objective robust optimisation of the sustainable helical milling process of the aluminum alloy Al 7075 using the augmented-enhanced normalised normal constraint method. J. Clean. Prod. 152, 474–496.
Rodriguez-Galiano, V., Sanchez-Castillo, M., Chica-Olmo, M., Chica-Rivas, M., 2015. Machine learning predictive models for mineral prospectivity: an evaluation of neural networks, random forest, regression trees and support vector machines. Ore. Geo.Rev. 71, 804–818.
Sarle, W.S., 1995. Stopped training and other remedies for overfitting. In: Proceedings of the 27th Symposium on the Interface of Computing Science and Statistics, pp. 352–360.
Shi, K.N., Ren, J.X., Wang, S.B., Liu, N., Liu, Z.M., Zhang, D.H., Lu, W.F., 2019. An improved cutting power-based model for evaluating total energy consumption in general end milling process. J. Clean. Prod. 231, 1330–1341.
Tian, C., Zhou, G., Zhang, J., Zhang, C., 2019. Optimization of cutting parameters considering tool wear conditions in low-carbon manufacturing environment. J. Clean. Prod. 226, 706–719.
Tong, Z., Miao, J., Tong, S., Lu, Y., 2021. Early prediction of remaining useful life for Lithium-ion batteries based on a hybrid machine learning method. J. Clean. Prod. 226, 706–719.
Wang, J., Fei, Z., Chang, Q., Li, S., 2019. Energy saving operation of manufacturing system based on dynamic adaptive fuzzy reasoning Petri net. Energies 12, 2216.
Wang, B., Liu, Z., Song, Q., Wan, Y., Shi, Z., 2016. Proper selection of cutting parameters and cutting tool angle to lower the specific cutting energy during high speed machining of 7050-T7451 aluminum alloy. J. Clean. Prod. 129, 292–304.
Wang, J., Zou, B., Liu, M., Li, Y., Ding, H., Xue, K., 2021. Milling force prediction model based on transfer learning and neural network. J. Intell. Manuf. 32, 947–956.
Wang, Y., Wen, Z., Li, H., 2020a. Symbiotic technology assessment in iron and steel industry based on entropy TOPSIS method. J. Clean. Prod. 260, 120900.
Wang, Z., Zhang, T., Yu, T., Zhao, J., 2020b. Assessment and optimisation of grinding process on AISI 1045 steel in terms of green manufacturing using orthogonal experimental design and grey relational analysis. J. Clean. Prod. 253, 119896.
Wimmer, S., Hunyadi, P., Zaeh, M.F., 2019. A numerical approach for the prediction of static surface errors in the peripheral milling of thin-walled structures. Prod. Eng. 13, 479–488.
Xu, L., Huang, C., Li, C., Wang, J., Liu, H., Wang, X., 2020. A novel intelligent reasoning system to estimate energy consumption and optimise cutting parameters toward sustainable machining. J. Clean. Prod. 261, 121160.
Xu, W., Jiang, C., Yan, L., Li, L., Liu, S., 2018. An adaptive Metropolis-Hastings optimisation algorithm of Bayesian estimation in non-stationary flood frequency analysis. Water Resour. Manag. 32, 1343–1366.
Xu, X., Meng, Z., 2020. A hybrid transfer learning model for short-term electric load forecasting. Electr. Eng. 102, 1371–1381.
Zhou, G., Lu, Q., Xiao, Z., Zhou, C., Yuan, S., Zhang, C., 2017. Ontology-based cutting tool configuration considering carbon emissions. Int.J. Precis. Eng. Man. 18, 1641–1657.
Zhu, K., Zhang, Y., 2019. A generic tool wear model and its application to force modeling and wear monitoring in high speed milling. Mech. Syst. Signal. PR. 115, 147–161.